

Report Documentation Page			Form Approved OMB No. 0704-0188		
Public reporting burden for the collection of information is estimated to average 1 hour per response, including the time for reviewing instructions, searching existing data sources, gathering and maintaining the data needed, and completing and reviewing the collection of information. Send comments regarding this burden estimate or any other aspect of this collection of information, including suggestions for reducing this burden, to Washington Headquarters Services, Directorate for Information Operations and Reports, 1215 Jefferson Davis Highway, Suite 1204, Arlington VA 22202-4302. Respondents should be aware that notwithstanding any other provision of law, no person shall be subject to a penalty for failing to comply with a collection of information if it does not display a currently valid OMB control number.					
1. REPORT DATE <b>2010</b>	2. REPORT TYPE		3. DATES COVERED <b>00-00-2010 to 00-00-2010</b>		
4. TITLE AND SUBTITLE <b>Characterization of a Fiber Optic Coupled Dosimeter for Clinical Electron Beam Dosimetry</b>			5a. CONTRACT NUMBER		
			5b. GRANT NUMBER		
			5c. PROGRAM ELEMENT NUMBER		
6. AUTHOR(S)			5d. PROJECT NUMBER		
			5e. TASK NUMBER		
			5f. WORK UNIT NUMBER		
7. PERFORMING ORGANIZATION NAME(S) AND ADDRESS(ES) <b>Oregon State University, Corvallis, OR, 97331-4501</b>			8. PERFORMING ORGANIZATION REPORT NUMBER		
9. SPONSORING/MONITORING AGENCY NAME(S) AND ADDRESS(ES)			10. SPONSOR/MONITOR'S ACRONYM(S)		
			11. SPONSOR/MONITOR'S REPORT NUMBER(S)		
12. DISTRIBUTION/AVAILABILITY STATEMENT <b>Approved for public release; distribution unlimited</b>					
13. SUPPLEMENTARY NOTES					
14. ABSTRACT					
15. SUBJECT TERMS					
16. SECURITY CLASSIFICATION OF:			17. LIMITATION OF ABSTRACT <b>Same as Report (SAR)</b>	18. NUMBER OF PAGES <b>57</b>	19a. NAME OF RESPONSIBLE PERSON
a. REPORT <b>unclassified</b>	b. ABSTRACT <b>unclassified</b>	c. THIS PAGE <b>unclassified</b>			

AN ABSTRACT OF THE THESIS OF

Kevin Dave Nitzling for the degree of Master of Science in Medical Physics presented on April 29, 2010.

Title: Characterization of a Fiber Optic Coupled Dosimeter for Clinical Electron Beam Dosimetry.

Abstract approved:

---

Camille J. Lodwick

Fiber-optic-coupled dosimeters (FOCDs) are a relatively new method in which to obtain *in-vivo* dose concomitant with radiation treatment. Accurate live dosing can be achieved virtually anywhere due to their small dimensions (0.2 mm) which can be accommodated by a catheter. The purpose of this experiment is to characterize the electron response of FOCDs with the intent of commissioning a total skin electron therapy (TSE) program.

The FOCD system, created by Brian Justus and Alan Huston at the Naval Research Laboratory in Washington, D.C., are composed of copper-doped fused quartz coupled to an optical fiber. The scintillation properties of the copper atoms make it an attractive element to use in radiation therapy based on the current pulse properties of most linear accelerators (linac).

System linearity, reproducibility, energy, output dependence on dose rate, field size, and cable effect were characterized at 6, 9, 12, 16 and 20 MeV electron energy ranges. The FOCDs demonstrated excellent linearity with an  $R^2$  value of 1.00,

electron energy dependence within  $\pm 1.67\%$  and the reproducibility of the FOCD system was within  $\pm 0.55\%$  for all energies in comparison to a reference ionization chamber, but fell short in the TSE commissioning process. The FOCDs exhibited a drop in signal when not positioned directly within the beam. The most likely cause for the dropped signal is due to its small cross-sectional area, rendering the system insensitive to scatter radiation. The results did, however, suggest that the FOCDs could prove highly valuable to integrate real-time *in-vivo* dose information concurrent with clinical electron radiation therapy.

©Copyright by Kevin Dave Nitzling  
April 29, 2010  
All Rights Reserved

CHARACTERIZATION OF A FIBER OPTIC COUPLED DOSIMETER FOR  
CLINICAL ELECTRON BEAM DOSIMETRY

by  
Kevin Dave Nitzling

A THESIS  
submitted to  
Oregon State University

in partial fulfillment of  
the requirements for the  
degree of

Master of Science

Presented April 29, 2010  
Commencement June 2010

Master of Science thesis of Kevin Dave Nitzling  
presented on April 29, 2010.

APPROVED:

---

Major Professor, representing Medical Physics

---

Head of the Department of Nuclear Engineering and Radiation Health Physics

---

Dean of the Graduate School

I understand that my thesis will become part of the permanent collection of Oregon State University libraries. My signature below authorizes release of my thesis to any reader upon request.

---

Kevin Dave Nitzling, Author

## ACKNOWLEDGEMENTS

I would first like to thank Brian Justus, Ph.D. and Alan Huston, Ph.D. at the Naval Research Laboratory in Washington, D.C., who worked diligently on updating the fibers during one of the worst snow storms in history, without their aid, this project would not have happened.

Special thanks to my advisor, Camille J. Lodwick, Ph.D. for her aid in the chaotic process that has surrounded my work. Because of you, I gained an understanding of Radiation Oncology and had the special privilege of being one of the first to major in medical physics at Oregon State University and pursue my true calling in life. Thank you for the opportunities that you have provided me, I will always be grateful.

I would like to thank the staff at Oregon Health and Sciences University for allowing me access to your department and providing the necessary support to carry out the data collection for this project.

Thanks to James Tanyi, Ph.D., especially his wife for allowing him to leave at all hours of the night to support this project. Through his guidance and tutelage I gained a greater insight into the fundamental aspects of Radiation Oncology. Because of you I now have an appreciation for the time-consuming work that goes on behind the scenes by the Medical Physicists when the clinic doors close.

Thank you to all of my friends and colleagues who have helped me in these past two years. I would especially like to thank Gordon Tannahill and Matt Asay, who

provided me sanity during the tough times, without their help I would not be where I am today.

Lastly, I would like to thank my family and friends who have provided me with support during this endeavor. To my wife Stefanie, who had to endure the sacrifice of staying at home with two young children without a means of transportation. It is because of your support that I was able to accomplish this endeavor. I love you more than these words can show, you are my lifeline and I thank you for all that you do.

## TABLE OF CONTENTS

	<u>Page</u>
CHAPTER 1 .....	1
INTRODUCTION .....	1
CHAPTER 2 .....	4
FIBER OPTICS .....	4
History of Fiber Optics .....	4
The Electromagnetic Spectrum .....	6
Refractive Index .....	7
Numerical Aperture .....	9
CHAPTER 3 .....	10
OPERATING PRINCIPLES .....	10
Scintillation .....	10
Activators .....	11
Cerenkov Radiation .....	12
Photomultiplier Tube .....	12
Linear Accelerator .....	14
CHAPTER 4 .....	16
MATERIALS AND METHODS .....	16
Linear Accelerator .....	16
Gated Fiber-Optic-Coupled Dosimeter .....	17
Farmer Chamber .....	20
Phantoms .....	21
Total Skin Electron Therapy (TSE) .....	21
Measurement Setup .....	22
Electron Dose Rate Dependence .....	22
Electron Energy Dependence .....	23
Electron Linearity .....	23

## TABLE OF CONTENTS CONTINUED

	<u>Page</u>
Electron Reproducibility .....	23
Electron Field Size Dependence .....	24
Electron Dose Per Pulse .....	24
Electron Cable Effect .....	24
TSE .....	25
CHAPTER 5 .....	27
RESULTS .....	27
Electron Dose Rate and Dose Per Pulse Dependence .....	27
Electron Energy Dependence .....	28
Electron Linearity .....	29
Electron Reproducibility .....	32
Electron Field Size Dependence .....	33
Electron Cable Effect .....	34
TSE Results .....	35
CHAPTER 6 .....	36
DISCUSSION .....	36
CONCLUSION .....	40
BIBLIOGRAPHY .....	42

## LIST OF FIGURES

<u>Figure</u>	<u>Page</u>
2-1. Electromagnetic Spectrum.....	7
2-2. Refraction and total internal reflection.....	8
3-1. Photomultiplier Tube.....	13
3-2. Block diagram of a Linear Accelerator.....	14
4-1. Varian Linear Accelerator (linac).....	16
4-2. Gated fiber-optic-coupled dosimeter (FOCD).....	17
4-3. Copper doped quartz fiber.....	18
4-4. The prototype gated fiber-optic-coupled dosimetry system setup.....	19
4-5. Farmer Ionization Chamber.....	20
4-6. TSE Commissioning Setup.....	26
5-1. Electron Dose Per Pulse.....	27
5-2. Electron Dose Rate Dependence.....	28
5-3. Electron Energy Dependence.....	29
5-4. Electron 6 MeV Linearity.....	30
5-5. Electron 9 MeV Linearity.....	30
5-6. Electron 12 MeV Linearity.....	31
5-7. Electron 16 MeV Linearity.....	31
5-8. Electron 20 MeV Linearity.....	32
5-9. Reproducibility of 100 MU doses from a 6 MeV beam.....	37

## LIST OF TABLES

<u>Table</u>	<u>Page</u>
5-1. Electron Reproducibility from 6 – 20 MeV.....	33
5-2. Output factors measured with a reference ionization chamber and three fiber-optic-coupled dosimeters in a solid water phantom.....	34

# CHAPTER 1

## INTRODUCTION

Rapid changes in technology have played a major role in the treatment of cancer using radiation. Yet with technological advances there is an ever increasing need to ensure accurate dose to patients. In January 2010, the New York Times reported that the average dose of diagnostic radiation has increased sevenfold since 1980, and more than half of all cancer patients receive radiation therapy (Bogdanich, 2010). The number of radiation mishaps in the recent past has garnered the attention of Congress leading to an inquiry with the American Association of Physicists in Medicine (AAPM). The need to accurately obtain patient *in vivo* dose information in real-time is an area that needs to be further researched to help minimize radiation mishaps in the future.

*In vivo* dosimetry could potentially play a crucial role in radiotherapy quality assurance by allowing for assessment of random and/or systematic deviations, essentially revealing uncertainties between prescribed and administered radiotherapy doses. The most commonly used *in vivo* patient dosimetry systems include thermoluminescence dosimeters (TLDs), silicon diodes, and metal oxide semiconductor field effect transistors (MOSFETs). Unlike TLDs that are not coupled to a signal processing system, diodes have the advantage of providing real-time feedback of accumulated dose. Diodes however, must be corrected for direction,

dose rate, dose per pulse, temperature and field size response dependence (AAPM Report 87, 2005). Furthermore, compensatory energy-dependent buildup required in diode manufacturing renders them bulky to the extent that they may perturb the electron fluence. Mitigating the drawbacks of the diode system has favored MOSFETs (Thomas et al., 1984) as a favorable alternative for clinical radiation therapy quality assurance. However, the drawback to MOSFETs is their relatively short life span, directional and energy response dependence, and need for frequent recalibration (Cheung et al., 2009).

To overcome the shortfalls of TLD, diode, and MOSFET dosimetry systems, a recent approach to *in vivo* dosimetry involves the utilization of ultra-small probes consisting of near tissue-equivalent plastic scintillators connected to optical fibers (Gasa, et al., 2006). Widespread adoption of plastic scintillators in clinical radiotherapy has been hindered by the difficulty of eliminating unwanted signal from Cerenkov radiation. Researchers have recently proposed techniques to mitigate or eliminate the undesirable effects of Cerenkov light including background subtraction temporal avoidance, and chromatic separation (Beddar et al., 1992, Fontbonne et al., 2002, Archambault, et al., 2006) which has renewed interest in this technology (Benevides, et al., 2007, Tanyi et al., 2010).

In the current study, a gated copper ion ( $\text{Cu}^+$ )-doped silica fiber optic coupled dosimeter (FOCD) is assessed using a linear accelerator (linac) and clinical electron energies with the intent of commissioning an electron total skin irradiation (TSE)

program. The unique properties of  $\text{Cu}^+$ -doped silica permit novel solutions to issues encountered by plastic scintillator dosimeters, such as low light collection efficiency and limitations due to Cerenkov emission (Justus et al., 2004). A systematic investigation of dosimetric characteristics including dose linearity, reproducibility, dose rate dependence, dose per pulse, electron energy and field size of the gated  $\text{Cu}^+$ -doped FOCD system to clinical radiotherapy electron beams is presented. Justus et al. (2004) demonstrated that the  $\text{Cu}^+$ -doped FOCD system is reliable for performance in a clinical setting for photons in the range of 6 – 15 MV. However, minimal studies have been performed using clinical electron energies in radiation therapy. Directional response of the dosimeter has been described (Benavides et al., 2007) and is beyond the scope of the current investigation. Furthermore, long-term stability and changes in response due to radiation damage were not examined.

The procedures in this experiment were performed in accordance with AAPM's Report No. 13 *Physical Aspects of Quality Assurance in Radiation Therapy* guidelines for acceptance testing of a new clinical dosimeter. The characterization of the FOCD allowed for direct comparison with a reference ionization chamber. The FOCD was then used in an effort to commission an electron total skin therapy (TSE) program in accordance with AAPM Report No. 23.

## **CHAPTER 2**

### **FIBER OPTICS**

#### **2.1 History of Fiber Optics**

Fiber optics can be traced back to Daniel Colladon, who, in 1841 showed that light can be guided through a water tank and out a jet on the other side (Hecht, 1999). The light rays underwent total internal reflection, which trapped the light in the water until the jet broke up. Around the same time Jacques Babinet, a specialist in optics at the French Academy of Sciences, performed a similar experiment using candlelight and a glass bottle. Babinet focused candlelight along the bottom of the bottle while pouring out a thin stream of water, watching as the internal reflection of the light illuminated objects at the end of the stream. Babinet further hypothesized that glass could be used as a conduit for light, but was unable to perform the experiment due to technological limitations (Hecht, 1999).

Thirteen years after Colladon had publically demonstrated total internal reflection John Tyndall a professor at the Royal Institution in London gained popularity for lectures and demonstrations with internal reflection through a fluid. The idea came from Tyndall's mentor, Michael Farraday, who was believed to have seen the experiment performed by Colladon. The original pioneers of fiber optics credited Tyndall and not Colladon for the light guiding in a water jet (Hecht, 1999).

In 1880, an American by the name of William Wheeler patented an invention for household lighting by guiding light using an electric arc that would be placed in the

basement. His experiment was made up of hollow glass pipes that were clear on the inside, coated with silver, and encased with asphalt to prevent any damages from scratches and tarnish. The invention worked, not by total internal reflection, rather by the reflection of light hitting the clear glass surfaces at a glancing angle in air (Hecht, 1999). Solid rods available for use at the time did not allow the possibility of carrying light throughout a house.

The use of glass for medical applications became of interest to many scientists, and effort was focused on establishing technology allowing dentists and physicians to peer into the throat of a patient. A German medical student by the name of Heinrich Lamm was interested in building a flexible gastroscope using a bundle of flexible fibers (Hecht, 1999). Lamm concluded that if all of the glass fibers were properly arranged so that they sat corresponding points at each end (a “coherent” bundle), then an image should be viewable from the opposite side of the bundle. Despite the poor image quality Lamm tried to patent his idea, and found that the concept was already patented by the Marconi Company in Britain. Still, Lamm became the first to transmit a crude fiber-optic image in 1930.

Lamm’s bundle concept was novel although he did not persist to investigate the cause of the poor image quality. He would have discovered that light was escaping the glass, which could be prevented if properly coated with a material having a lower index of refraction than glass. In 1956 an undergraduate student by the name of Larry Curtiss constructed a fiber from a glass tube collapsed upon a glass rod. This set about

a series of events, and the gastroscope that Lamm had originally tried to make was patented in 1956 by Basil Hirschowitz, William Peters and Curtiss. The science of fiber optics has grown immensely since 1956 and optical fibers are currently heavily used in communications to transmit data over long distances and at high bandwidths. Optical fibers have much lower attenuation and much higher bandwidth than metallic wires or coaxial cables. Additionally, since fibers are insulators, they are not susceptible to electromagnetic interference as are metallic conductors (Hecht, 1999).

## 2.2 The Electromagnetic Spectrum

The electromagnetic spectrum (Figure 2-1) consists of electric and magnetic field components that oscillate in phase perpendicular to each other and perpendicular to the direction of energy propagation. Electromagnetic radiation is generally classified according to the frequency of its wave, including: radio waves, microwaves, infrared radiation, visible light, ultraviolet radiation, X-rays and gamma rays. Optical fibers function in the visible and near infrared frequency range which corresponds to wavelengths between 400 and 1500 nm. The wavelength is inversely proportional to the frequency and is defined as:

$$\text{wavelength } (\lambda) = \frac{\text{speed of wave } (v)}{\text{frequency } (f)}$$

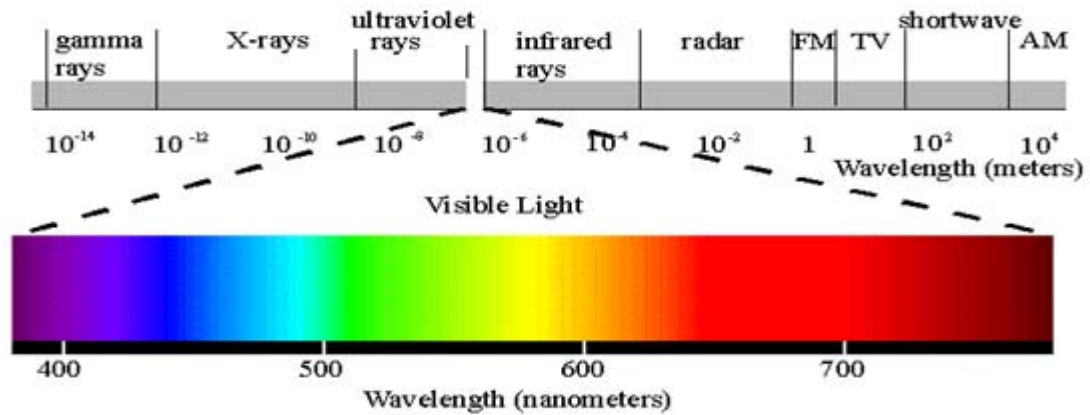


Figure 2-1. Electromagnetic Spectrum.

## 2.3 Refractive Index

The refractive index is the ratio of the speed of light in a vacuum and the speed of light in the medium.

$$n = \frac{\text{speed of light in a vacuum } (c)}{\text{speed of light in medium } (v)}$$

Light traveling in a medium is always slower than light traveling in a vacuum, making values for the index of refraction greater than 1.0. When a light beam impinges at an angle on a surface with a different refractive index, the light is bent from the incident path (figure 2-2). The angle at which the light is transmitted,  $\theta_2$ , depends on the refractive index of the two materials and the angle of the incident light to the surface between them,  $\theta_1$ . This is described by Snell's law.

$$n_1 \sin \theta_1 = n_2 \sin \theta_2$$

where  $\theta_1$  is the angle from normal to the interface of the incident ray and  $\theta_2$  is the angle of transmission in medium 2.

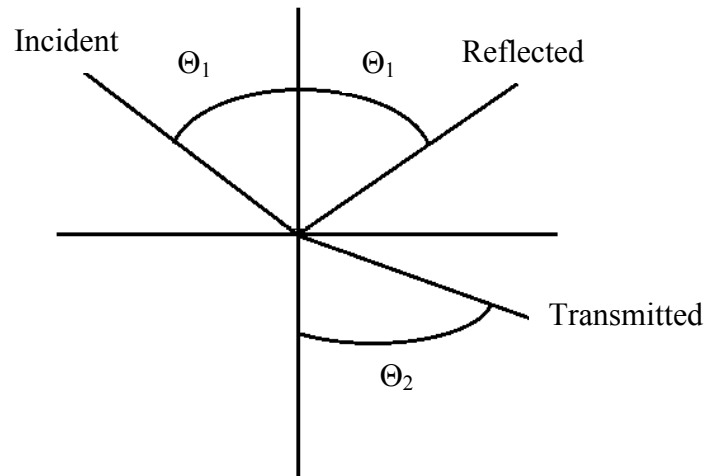


Figure 2-2. Refraction and total internal reflection.

Snell's law indicates that light escape out of the glass fiber optic medium if the angle of incidence is less than the “critical value”. The critical value is when the incident angle results in a  $90^\circ$  angle of refraction of the transmitted ray, resulting in no transmission. The critical angle, derived using Snell's law is:

$$\theta_{critical} = \arcsin\left(\frac{n_2}{n_1}\right)$$

$n_2$  is the refractive index of the less optically dense medium and  $n_1$  is the refractive index of the more optically dense medium. Total internal reflection is when  $\theta_{incident} > \theta_{critical}$ .

## 2.4 Numerical Aperture

Numerical Aperture (NA) is defined as the sine of the maximum angle of incident light on the end of the fiber that will be captured by total internal reflection in the fiber core and is defined as:

$$NA = \sin^{-1} \theta_{max} = \sqrt{n_1^2 - n_2^2}$$

where  $n_1$  is the refractive index of the core and  $n_2$  is the refractive index of the cladding. Fibers with larger NAs can capture more light into their cores. Light rays will be guided along the core according to the acceptance angle, which is measured in air outside of the fiber. The acceptance angle differs from the confinement angle within the glass fiber.

## **CHAPTER 3**

### **OPERATING PRINCIPLES**

#### **3.1 Scintillation**

Scintillation is a flash of light that is produced by a phosphor when it absorbs a photon or ionizing radiation. There are six properties that an ideal scintillation material should have (Knoll, 2000):

1. It should convert the kinetic energy of charged particles into detectable light with a high scintillation efficiency.
2. The light yield should be proportional to deposited energy over as wide a range as possible.
3. The medium should be transparent to the wavelength of its own emission for good light collection.
4. The decay time of the induced luminescence should be short so that fast signal pulses can be generated.
5. The material should be of high optical quality that can be fabricated in sizes large enough for use in a practical detector.
6. The index of refraction should be near that of glass (about 1.5) to permit efficient coupling of the scintillation light to a photomultiplier tube or other light amplification sources.

Light output of a phosphor is due to one of two mechanisms fluorescence and phosphorescence. Fluorescence is the luminescence that is caused by the absorption of radiation at one wavelength followed by nearly immediate re-radiation usually at a longer wavelength and that ceases rapidly ( $\sim 10$  ns) when the incident radiation stops. Phosphorescence is similar to fluorescence but proceeds via slower metastable energy transitions and has a characteristic time that is generally much slower (msecs – hours) (Knoll, 2000).

### **3.2 Activators**

Scintillation in organic materials is dependent on the number of energy states within their crystal lattices. Discrete energy bands exist in materials classified as insulators or semiconductors. The valence band is the lower energy state and is representative of the electrons that are bound at lattice sites. In semiconductors electrons that overcome the band gap energy to reach the conduction band are free to move throughout the crystal. An intermediate, “forbidden”, band is a region in which no electron states exist. In a pure crystal, the absorption of energy elevates an electron from the valence band across the forbidden region into the conduction band, leaving behind a hole in the valence band. The return of an electron back to the valence band in a pure crystal is an inefficient process. Typical gap widths are such that the resulting photon would be outside the visible range (Knoll, 2000).

Therefore, to increase the probability of emitting a visible photon during the de-excitation process, a small amount of impurities known as activators are added to the

inorganic scintillators. These activators modify the crystal lattice creating electron trapping centers within the forbidden gap. The energy state of these induced electron traps is such that de-excitation to the valence band produces a visible photon, which is the basis of the scintillation process (Knoll, 2000).

### **3.3 Cerenkov Radiation**

Cerenkov radiation is generated in optical fibers when charged particles enter the core with a velocity greater than the local phase velocity of light. The intensity of the Cerenkov light is strongly dependent on the angle between the optical fiber axis and the particle trajectory, reaching a maximum when the Cerenkov cone is directed along the axis of the fiber (S.H. Law et al., 2006, 2007). In radiotherapy applications Cerenkov light can exceed the intensity of the scintillation signal, even at the most intense scintillation wavelength (Lambert, et al., 2009).

### **3.4 Photomultiplier Tube**

The scintillation signal is only useful if accompanied by a means to measure the scintillation intensity; hence, the purpose of the photomultiplier (PM) (Figure 3-1). The PM tube consists of an outer shell typically made of glass that serves as a pressure boundary to sustain vacuum conditions inside the tube. A vacuum is required to provide efficient acceleration of low-energy electrons without attenuation by internal electric fields.

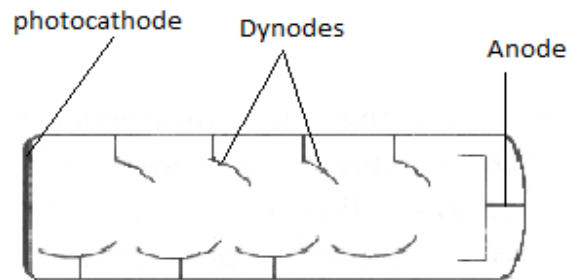


Figure 3-1. Photomultiplier Tube (PMT).

A photocathode is at the entrance of the PM tube and directly converts a fraction of the incident light photons into low-energy electrons (1 eV or less) via the photoelectric effect. Therefore, the number of electrons created will be proportional to the entering photon intensity. The low-energy electrons are guided towards a series of dynodes, each containing a higher voltage than the previous to attract the incoming electrons in a chain which ends at the anode. The creation of an excited electron within the dynode requires a minimum energy equal to the bandgap, which may be on the order of 2-3 eV. The electrons are collected at the anode, which is the output stage of the PM tube. The multiplication factor for each dynode is given by the following formula and should be large to maximize total amplification of the PM tube:

$$\delta = \frac{\text{number of secondary electrons emitted}}{\text{primary incident electron}}$$

### 3.5 Linear Accelerator

A linear accelerator (linac) is a radiotherapy machine that uses high-frequency electromagnetic waves to accelerate electrons to high energies through a linear tube (Khan, 2003). Because the functionality directly relates to the operation of the FOCD system, it is important to understand the linac. Figure 3-2 illustrates the basic components of the linac.

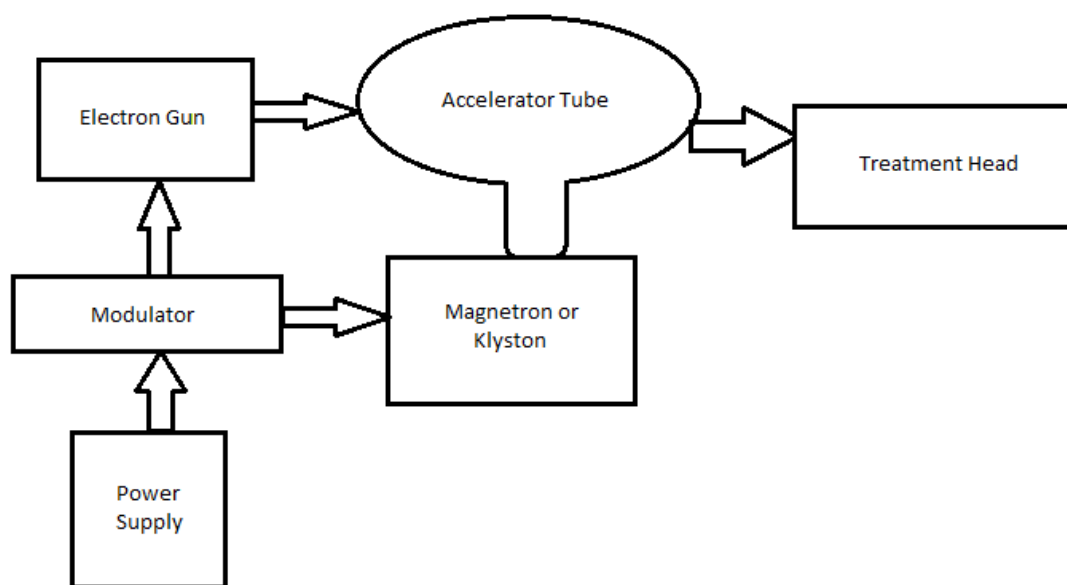


Figure 3-2. Block diagram of a Linear Accelerator.

The power supply provides direct current (DC) power to the modulator, which includes the pulse-forming network and a switch tube known as a thyatron. High voltage pulses from the modulator are flat-topped DC pulses of a few microseconds in duration. The pulses are delivered to the klystron (produce microwaves) and

simultaneously to the electron gun. Pulsed microwaves produced in the klystron are injected into the accelerator tube via a waveguide system. These pulses are several microseconds in duration and repeat at a rate of several hundred pulses per second. Electrons, produced by an electron gun are also simultaneously injected into the accelerator structure (Khan, 2003).

The accelerator structure consists of a copper tube with its interior divided by copper discs or diaphragms of varying aperture and spacing, and is evacuated to a high vacuum. The electrons are injected into the accelerator structure with an initial energy of around 50 keV, and gain energy via interactions with the electromagnetic fields. The electrons emerge in a narrow beam of about 3 mm in diameter, which is magnetically bent to produce a monoenergetic beam of electrons. The filtered electrons either hit a tungsten target to create x-rays or strike a scattering foil to spread the beam to a larger treatment area (Khan, 2003).

## CHAPTER 4

### MATERIALS AND METHODS

#### 4. 1 Linear Accelerator

A Varian Trilogy radiotherapy linear accelerator (figure 4-1) was used to provide 6, 9, 12, 16, 20 MeV electrons at dose rates between 100 and 1000 monitor units (MU) for electrons and between 100 and 600 MU/min for photons. The output of the linear accelerator is a train of pulses, each typically  $\sim 5 \mu\text{s}$  wide. The pulse repetition rate varies between  $\sim 50 \text{ Hz}$  and  $\sim 600\text{Hz}$ : as such, the time interval between electron pulses varies from  $\sim 20 \text{ ms}$  (corresponding to the machine dose rate of 1000 MU/min). (Tanyi, 2010).

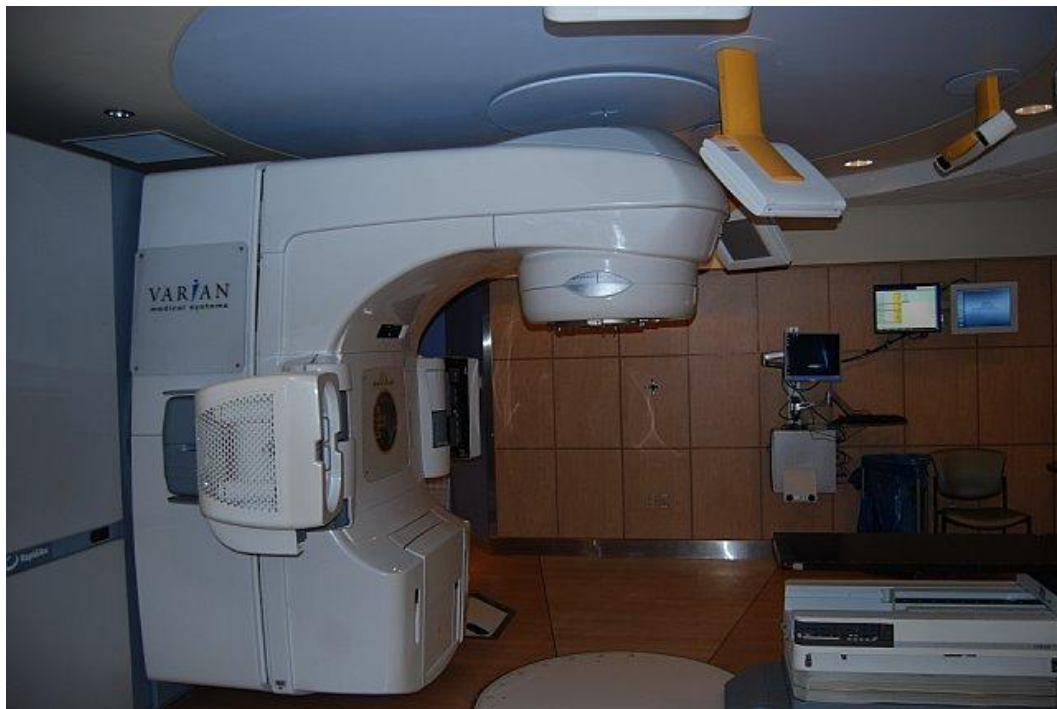


Figure 4-1. Varian Linear Accelerator (linac).

## 4.2 Gated Fiber-Optic-Coupled Dosimeter

The gated fiber-optic-coupled dosimeter characterized in this work was developed by Brian Justus and Alan Huston at the Naval Research Laboratory in Washington D.C. (figure 4-2). The system is comprised of three radiation sensitive elements fabricated by the doping of fused-quartz glass with  $\text{Cu}^{1+}$  ions.



Figure 4-2. Gated fiber-optic-coupled dosimeter (FOCD).

The doped quartz pre-form was drawn into the fiber, and a short length ( $\sim 5\text{cm}$ ) of the fiber was attached to a 1m length of multimode optical fiber ( $400\text{ }\mu\text{m}$  core diameter) by use of a plasma fusion fiber splicer. The fused fiber was then cleaved, yielding a radiation sensitive point detector at the end of the fiber 1 mm long and  $400\text{ }\mu\text{m}$  in diameter corresponding to a volume of about  $3 \times 10^{-4}\text{ cm}^3$  (Figure 4-3). The copper doped quartz scintillator with 1 mm of silica fiber was then attached to a silica optical fiber waveguide by the plasma fusion method (Justus et. al., 2004). There were no

significant losses upon coupling of the light from the quartz dosimeter fiber into the silica optical fiber (Justus et. al., 2004).

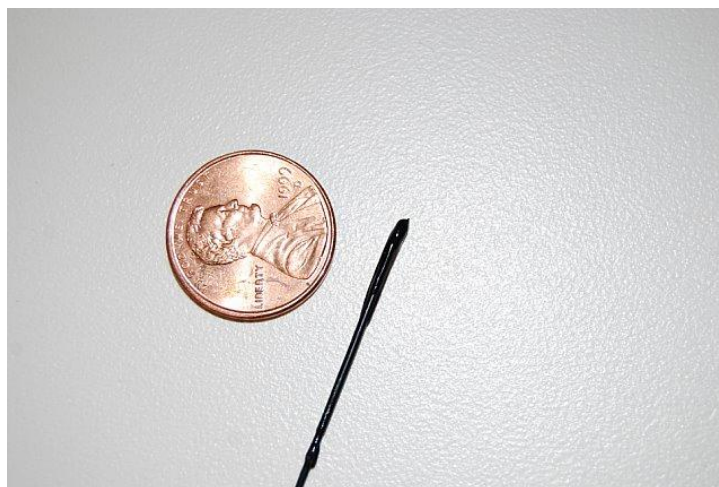


Figure 4-3. Copper doped quartz fiber.

The silica optical fiber waveguide was attached to a 15 m fiber-optic patch cord to reach the readout unit. The patch cords were coupled to the input window of a photon-counting photomultiplier tube (PMT) module (Hamamatsu H-6240-01). The transistor-transistor logic (TTL) output pulses from the PMT module interfaced with a high-precision 32-bit counter. The counted sums are then transferred into a buffer on each edge of the gate pulse (rising and falling) (Justus, et al., 2004).

A trigger detector was used to detect scattered photons in order to provide a gate synchronization signal. The scattered-photon detector utilizes a  $\sim 10 \times 2.5 \times 2 \text{ cm}^3$  plastic scintillator (Saint-Gobain BC-408) coupled directly to the face of a PMT (Hamamatsu HC124-03). The scattered photon detector was placed at  $\sim 4 \text{ m}$  from the source, Figure 4-4.

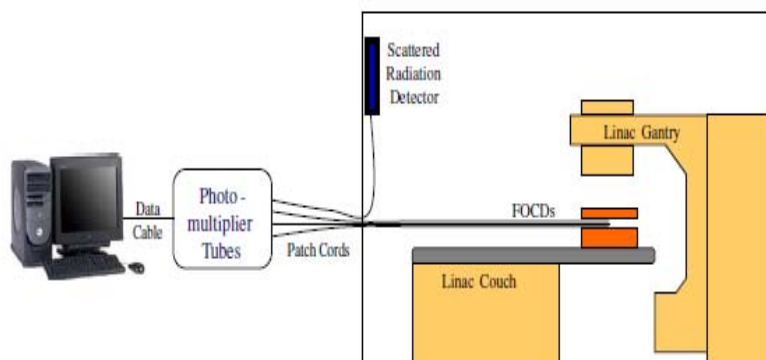


Figure 4-4. Gated fiber-optic-coupled dosimetry system setup (Courtesy of Tanyi et al. 2010).

The decay characteristics of the  $\text{Cu}^{+1}$  doped luminescence can be utilized in radiation therapy. The decay of the photoluminescence is characterized by two exponentials due to the superposition of decay of  $\text{Cu}^{1+}$  ions occupying multiple sites in the glass with decay times of 51 and 104  $\mu\text{s}$  (Justus et. al, 2004). The decay of the phosphorescence from  $\text{Cu}^{+1}$  doped glass after being excited by an x-ray pulse is similar. The time interval between x-ray pulses from the linac varies from 20 ms at 100 MU/min to about 2 ms at 1000 MU/min, so the phosphorescence from the dosimeter decays completely between pulses (Justus et. al, 2004).

While the linac is actively pulsing, the signal in each optical fiber includes both native luminescence, phosphorescence from the  $\text{Cu}^{+1}$  and Cerenkov radiation. However, in between pulses the light signal consists only of  $\text{Cu}^{+1}$  phosphorescence as the native signal decays on the scale of picoseconds and the native fluorescence decays on the order of nanoseconds. The phosphorescence from the  $\text{Cu}^{+1}$  lasts for

several hundred microseconds after the termination of the x-ray pulse (Justus et. al, 2004).

### 4.3 Farmer Chamber

Created in 1955 this ion chamber provides stable and reliable measurement standards for photon and electron beams in the therapeutic range. The thimble wall is fabricated with pure graphite and the central electrode is pure aluminum, the insulator consists of polytrichlorofluorethylene and the collecting volume of the chamber is  $0.6 \text{ cm}^3$ . An ion chamber consists of a central electrode for the signal collection, a thimble wall and a guard electrode. The collector delivers the current to an electrometer, which has a dual polarity high voltage source to hold the collector at a high bias voltage (300 V) (Khan, 2003). For this study a PTW N30004 ionization chamber (figure 4-5) and a PTW UNIDOS electrometer with calibrations traceable to an Accredited Dosimetry Calibration Laboratory (ADCL), were used to assess the validity of the FOCD response.



Figure 4-5. Farmer Ionization Chamber.

#### 4.4 Phantoms

For clinical use in radiation therapy a phantom must be made of material that is “tissue equivalent”. The closest tissue equivalent material is water, so any other material that is used, must have the same effective atomic number, number of electrons per gram, and mass density as water (Khan, 2003). The electron density ( $p_e$ ) can be calculated from a materials atomic composition and its mass density ( $p_m$ ) with the following formula:

$$p_e = p_m \times N_a \times \left( \sum_i a_i \times \left( \frac{Z_i}{A_i} \right) \right)$$

where  $N_a$  is Avogadro’s number,  $a_i$  is the fraction by weight of the  $i$ th element of atomic weight  $A_i$  and atomic number  $Z_i$ . For this study solid water (plastic) was used, which has a mass density of 1.00 g/cm<sup>3</sup> and the electron density of 3.34 x 10<sup>23</sup> electrons/gram, compared to water with a mass density of 1 g/cm<sup>3</sup> and 3.34 x 10<sup>23</sup> electrons/gram. A tissue-equivalent bolus material (0.5 cm thickness) was used to protect the fibers of the FOCD and served as a build-up material for measurements.

#### 4.5 Total Skin Electron Therapy (TSE)

Electrons between the energies of 2 to 9 MeV are useful in treating superficial lesions covering large areas of the body, like mycosis fungoides and other cutaneous lymphomas (Khan, 2003). This range of energies allows for treatment of lesions up to 1 cm depth without harming bone marrow. There are two main methods of treatment, translational and large field technique. This experiment focuses on commissioning the

large field technique. The large field technique for total body skin irradiation is done by scattering electrons through wide angles at a large distance from the linac.

Contamination from x-rays is an issue when performing therapy with an electron beam. Normally these x-rays are contributed by bremsstrahlung interactions that occur in the exit window of the linac, the scattering foil, ion chambers, air, patient and beam-defining collimators. The technique used in this study, is a modified Stanford technique in which the electron beam is collimated to a wide aperture by projecting the beam at 2 angles, each 20 degrees of the central axis with the gantry in the horizontal direction.

## **4.6 Measurement Setup**

The American Association of Physicists in Medicine (AAPM) Report No. 13 Physical Aspects of Quality Assurance in Radiation Therapy guidelines was used to characterize the FOCD and the reference PTW N30004 ionization chamber. The dosimeters were centered about the central axis of the beam port with a delivered dose of 1 cGy for 1 MU unless noted otherwise. All measurements listed below were performed using the reference PTW N30004 ionization chamber.

### **4.6.1 Electron Dose Rate Dependence**

Three FOCDs were irradiated with a 6 MeV electron beam at various dose rates to observe any change in their response. The linac delivered dose rates of 100, 200, 300, 400, 500, 600, and 1000 MU/min. The measurements at each dose rate were

performed five times and averaged. These averages were then normalized the measurement at 600 MU/min.

#### **4.6.2 Electron Energy Dependence**

Energy dependence was assessed using a 10 X 10 cm<sup>2</sup> cone size for 100 MUs at a machine dose rate of 600 MU/min for 6, 9, 12, 16 and 20 MeV electron beam energies. Measurements were performed at two depths for each energy: 1.2 cm and 2.0 cm for 6 MeV, 2.0 cm and 3.0 cm for 9 MeV, 3.0 cm and 4.0 cm for 12 MeV, 3.0 cm and 5.5 cm for 16 MeV, and 3.0 cm and 6.5 cm for 20 MeV. The energy of each beam was defined as an ionization ratio, computed by dividing an average of five measurements at the first depth to corresponding measurements at the second depth.

#### **4.6.3 Electron Linearity**

To determine the useful range of the FOCs, linearity was performed using a 10 X 10 cm<sup>2</sup> cone, a machine dose rate of 600 MU/min and a range of clinical doses: 6, 9, 12, 16 and 20 MeV. The monitor units were then varied between 1, 2, 3, 5, 10, 25, 50, 75, 100, 250, 500 and 1000 MU. Five measurements were recorded; the average was used to report the response of the FOCs for each dose and then normalized to the 100 MU responses for comparison with the response of the reference ionization chamber.

#### **4.6.4 Electron Reproducibility**

The reproducibility of FOC response was tested using 6, 9, 12, 16 and 20 MeV beam delivering 100 MU at a rate of 600 MU/min. A source to surface distance (SSD)

of 100 cm and a 10 X 10 cm<sup>2</sup> cone was used and all measurements were performed 25 times. The data was then averaged and the standard deviation calculated.

#### **4.6.5 Electron Field Size Dependence**

The total range of electrons (6, 9, 12, 16, 20 MeV) with a rate of 600 MU/min were used with cone sizes of 6 x 6, 10 x 10, 15 x 15, 20 x 20, 25 x 25 cm<sup>2</sup>. Build-up factors were used (in cm) of 1.2 (6 MeV), 2.0 (9 MeV) and 3.0 (12, 16, 20 MeV) to ensure that the optimal energy was deposited to the dosimeter. An SSD of 100 cm was used for each of the measurements. Five measurements were acquired for each energy and cone size, and then averaged. These averages were then normalized to the 10 x 10 cm<sup>2</sup> results and graphed.

#### **4.6.6 Electron Dose Per Pulse**

A 6 MeV beam was used with a rate of 600 MU/min (1.2 cm build-up) with SSDs of 100, 105, 110, 115, 120, 125 cm. The results were then normalized to the SSD 100cm values.

#### **4.6.7 Electron Cable Effect**

A 25 x 25 cm<sup>2</sup> cone (36 x 36 cm<sup>2</sup> field size), 100 SSD, a 6 MeV beam (1.2 cm build-up), for 100 MU at a rate of 600 MU/min. To test for any cable effect 12.5 cm of cable was placed directly in the field, then 55 cm of cable and 110 cm of cable to include the junction boxes. Five measurements were taken and then averaged.

#### 4.6.8 TSE

AAPM report 23 was used as the guidelines for the TSE commissioning. The setup included placing a parallel-plate ionization chamber into the solid phantom plate with no buildup plates on top of the chamber. The ionization chamber always faces the beam with a 300 V bias. Styrofoam was used to set the ionization chamber at different levels from the floor, with the same length of chamber cable exposed to beams in all measurements. A vertical distance of 200 cm was maintained between the ionization chamber and the isocenter for all measurements. The gantry was placed at 110, 90 and 70 degrees with measurements taken directly in and out of the beam to account for patient dose due to the beam and scatter radiation. All of the electron beams had zero collimator angle, respectively at Gantry 110, 90 and 70 degrees, and 300 MU were delivered for each gantry angle. Zero point is at the central axis of the beam with the gantry at 90° and is 200 cm from ISO), and all other points of measurements are in respect to it. The y-axis is vertical with the origin at the zero point and positive toward the ceiling and negative towards the floor. The x-axis is horizontal with the origin at the zero point and positive toward gantry. The z-axis is horizontal with the origin at the zero point and positive along beam axis at gantry 90°.



Figure 4-6. TSE Commissioning Setup.

## CHAPTER 5

### RESULTS

#### 5.1 Electron Dose Rate and Dose Per Pulse Dependence

Figure 5-1 shows the average dose rate dependence of the FOCD system at dose rates ranging from 100 to 1000 MU/min. The FOCD response was within  $\pm 0.50\%$  of reference ionization chamber measurements and remained uniform well within the reproducibility of the FOCD system. The relative response of the FOCDs and the reference ionization chamber is plotted against SSDs ranging from 100 – 125 cm for the 6 MeV electron beam (Figure 5-2). The FOCD response is within 0.51% of the reference ionization chamber measurements, except for measurements at 115 cm where the difference was 0.89%.

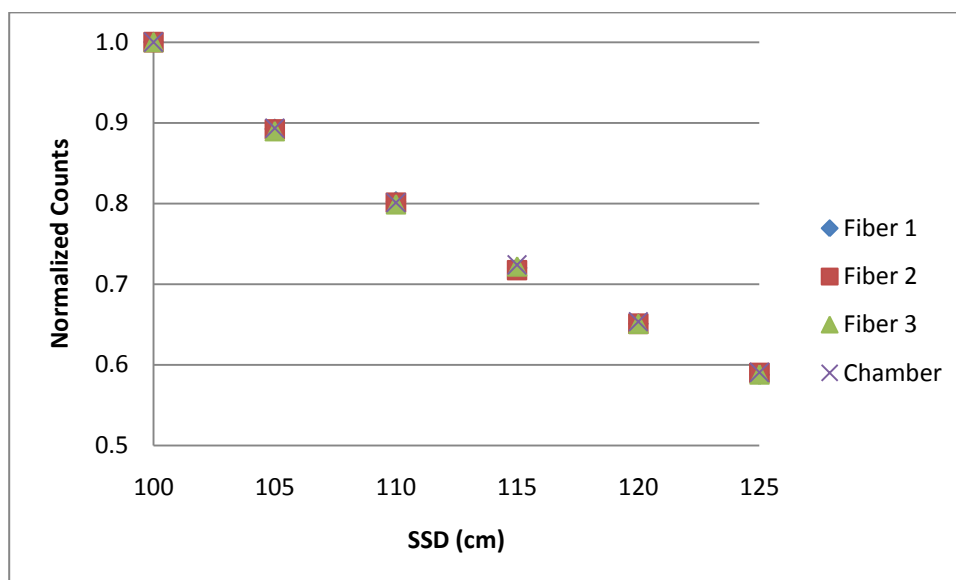


Figure 5-1. Electron Dose Per Pulse.

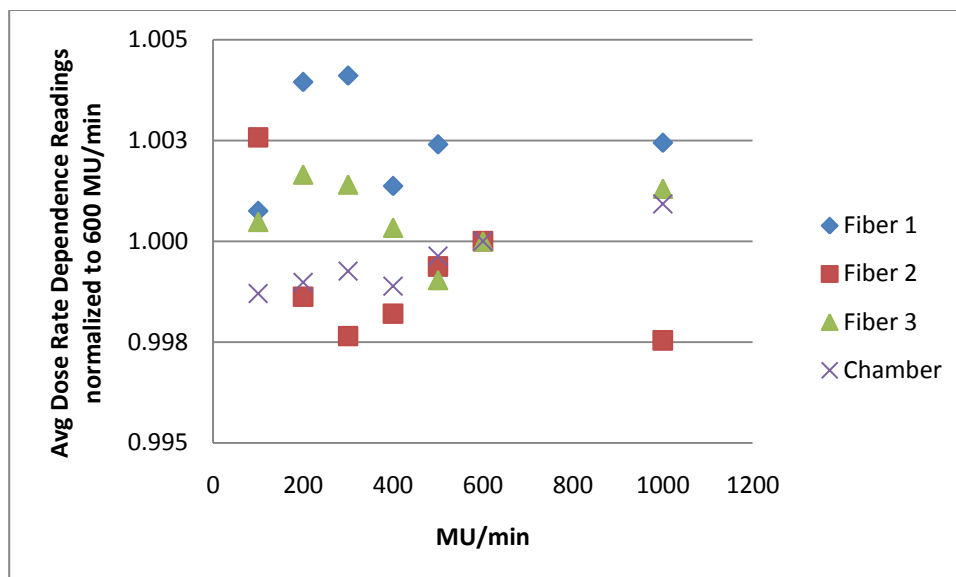


Figure 5-2. Electron Dose Rate Dependence.

## 5.2 Electron Energy Dependence

Figure 5-3 shows the energy response of the FOCD system for clinical electron beams in the range of 6–20 MeV. The ionization ratio of the FOCDs correlated well with that of the reference ionization chamber, and was within  $\pm 1.67\%$  for all the energies investigated, indicating little or no energy dependence.

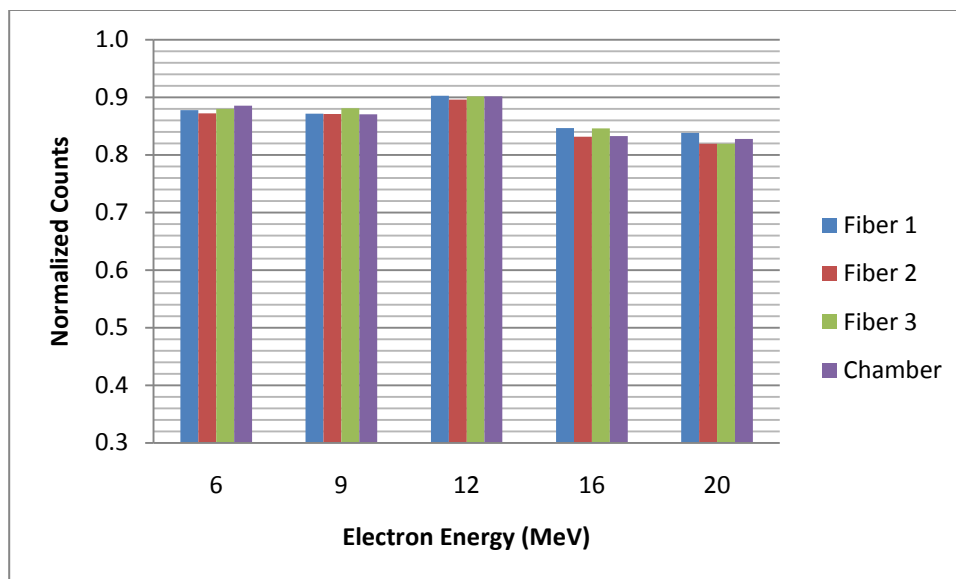


Figure 5-3. Electron Energy Dependence.

### 5.3 Electron Linearity

The response of the FOCD system was in excellent agreement with the reference ionization chamber measurements for doses ranging from 1 – 1000 cGy for electron beam energies in the range of 6–20 MeV (figures 5-4 to 5-8). The response of each FOCD to each electron beam energy was linear, with computed linearity coefficients with  $R^2$  value = 1.0.

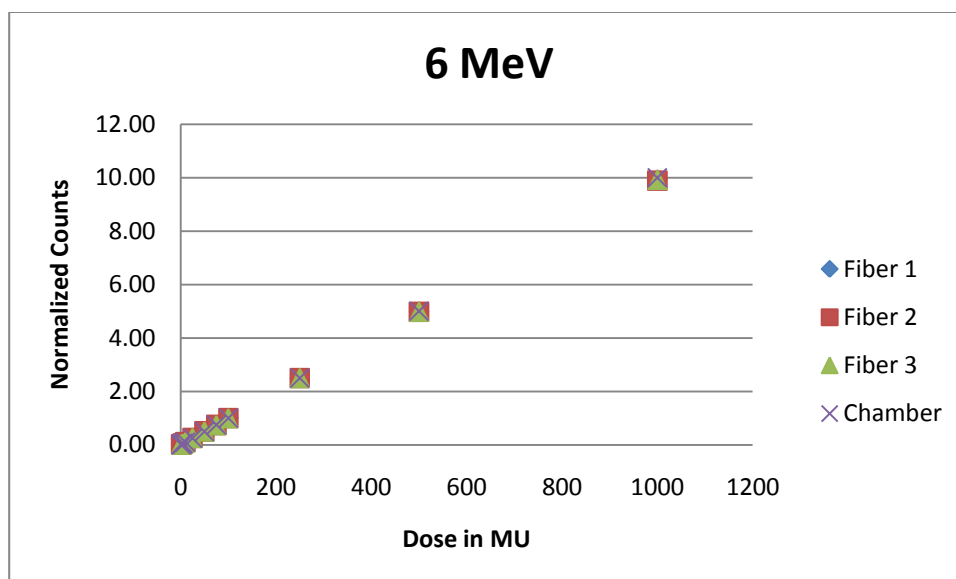


Figure 5-4. Electron 6 MeV Linearity.

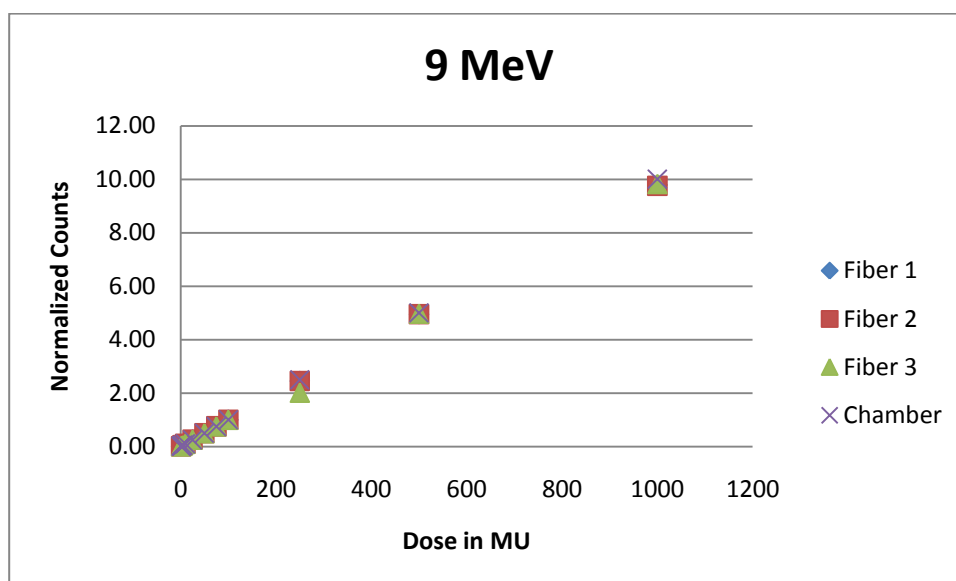


Figure 5-5. Electron 9 MeV Linearity.

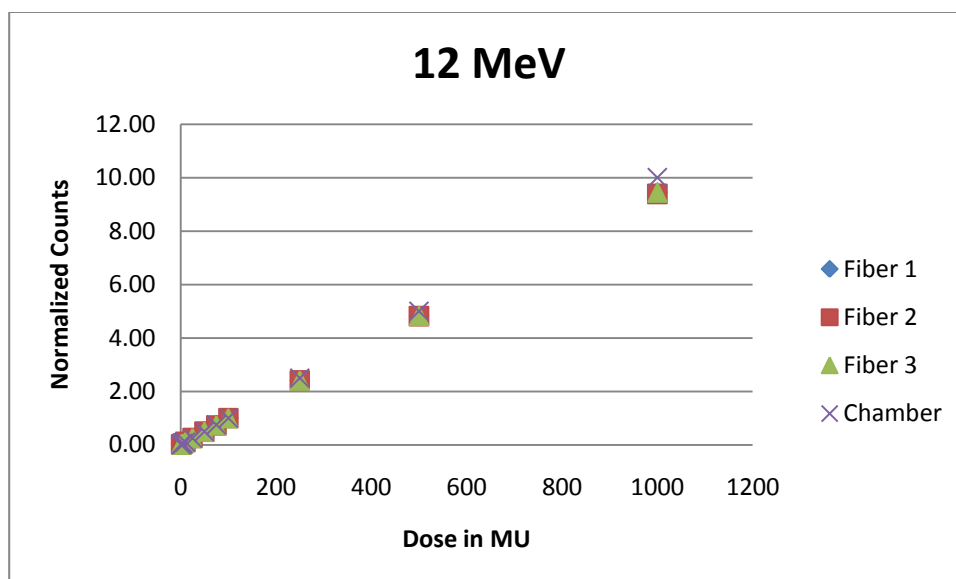


Figure 5-6. Electron 12 MeV Linearity.

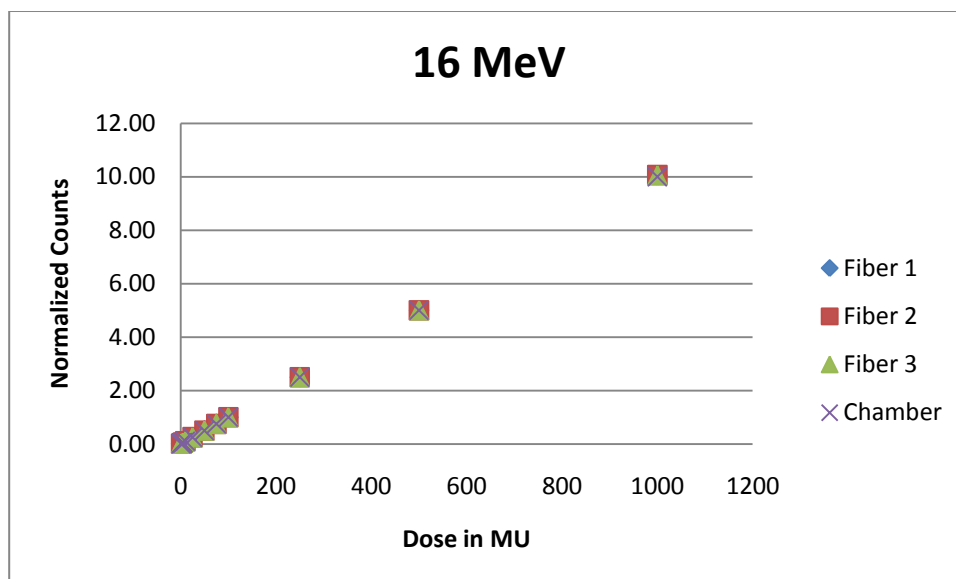


Figure 5-7. Electron 16 MeV Linearity.

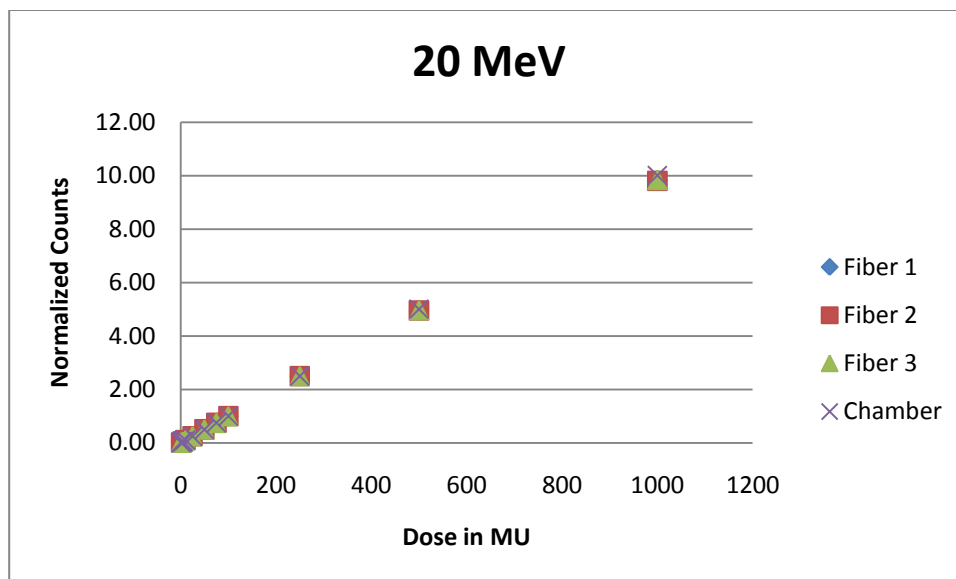


Figure 5-8. Electron 20 MeV Linearity.

#### 5.4 Electron Reproducibility

Figure 5-9 shows the reproducibility of the FOCD system in solid water at standard calibration setting for a 6 MeV electron beam at 100 MU irradiations. The reproducibility of the FOCD system was within  $\pm 0.55\%$  (see Table 5-1).

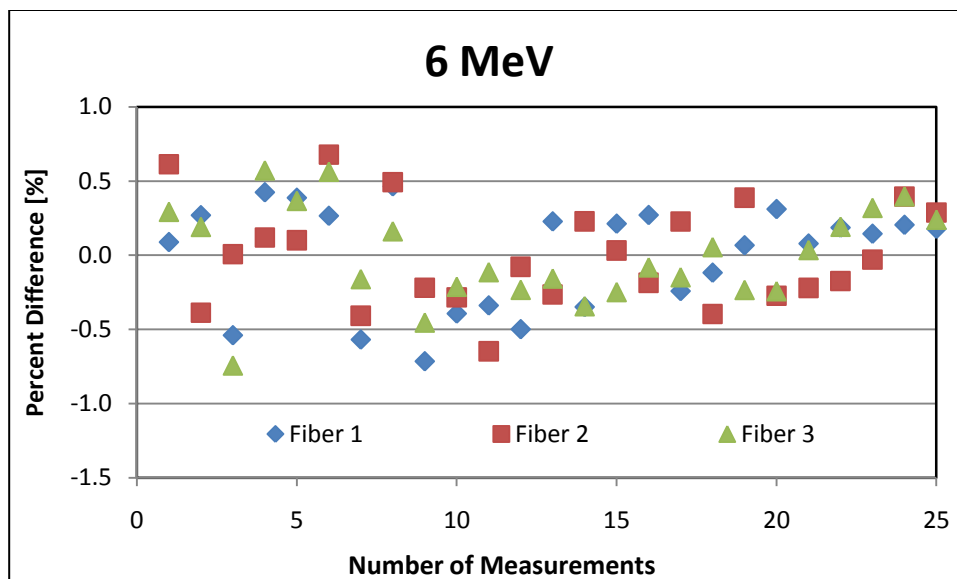


Figure 5-9. Reproducibility of 100 MU doses from a 6 MeV beam

Table 5-1. Electron Reproducibility from 6 – 20 MeV.

Energy (MeV)	Fiber 1	Fiber 2	Fiber 3
6	0.35	0.35	0.32
9	0.41	0.35	0.55
12	0.34	0.40	0.34
16	0.37	0.40	0.40
20	0.27	0.23	0.28

## 5.5 Electron Field Size Dependence

Table 5-2 shows a comparison of the output factors measured with each FOCD and the reference ionization chamber. The FOCD output factors were in good agreement with those of the reference ionization chamber. Quantitatively, the maximum

difference between the FOCD response and that of the reference ion chamber was within  $\pm 1.69\%$  (6 MeV),  $\pm 0.77\%$  (9 MeV),  $\pm 0.64\%$  (12 MeV),  $\pm 1.46\%$  (16 MeV), and  $\pm 1.55\%$  (20 MeV).

Table 5-2: Output factors measured with a reference ionization chamber and three fiber-optic-coupled dosimeters in a solid water phantom.

Field Size (cm <sup>2</sup> )	6 MeV		9 MeV		12 MeV		16 MeV		20 MeV	
	Chamber	FOCD	Chamber	FOCD	Chamber	FOCD	Chamber	FOCD	Chamber	FOCD
6	0.966	0.951	0.978	0.983	0.968	0.974	0.985	0.998	0.999	0.998
		0.949		0.983		0.972		0.997		1.000
		0.954		0.985		0.971		0.999		1.004
10	1.000	1.000	1.000	1.000	1.000	1.000	1.000	1.000	1.000	1.000
		1.000		1.000		1.000		1.000		1.000
		1.009		0.999		0.987		0.998		0.977
15	1.003	1.009	0.997	0.998	0.993	0.988	0.986	0.995	0.978	0.977
		1.011		0.996		0.989		0.997		0.982
		1.009		0.976		0.977		0.978		0.959
20	1.014	1.008	0.984	0.978	0.976	0.974	0.970	0.977	0.955	0.960
		1.009		0.979		0.980		0.981		0.965
		1.000		0.958		0.951		0.950		0.930
25	1.010	1.003	0.963	0.956	0.949	0.948	0.939	0.948	0.923	0.928
		1.005		0.960		0.949		0.950		0.938

## 5.6 Electron Cable Effect

There was a very noticeable cable effect when the patch cord connectors were directly in the electron beam. The patch cord connectors are not light tight and do contribute a significant amount of error when directly in the electron beam.

## **5.7 TSE Results**

The TSE commissioning could not be completed in its entirety, due to the FOCDs inability to accurately detect scatter electron measurements. When the FOCDs were not close to the central beam, signal was dropped and sufficient data could not be collected.

## CHAPTER 6

### DISCUSSION

During the last twenty years, there has been an increased interest in scintillation dosimetry using water-equivalent plastic scintillators with good spatial and temporal resolution and because of favorable characteristics including reproducibility, linearity of response with dose, dose-rate proportionality and energy independence, when compared with other more commonly used detector systems. Despite these desirable qualities, plastic scintillators have not reached their full potential for routine clinical applications in radiation oncology because of the limitations imposed by signal coupling inefficiencies and noise capture, mostly from Cerenkov radiation.

Cerenkov radiation is generated in optical fibers when charged particles enter the core with a velocity greater than the local speed of light. The intensity of the radiation is strongly dependent on the angle between the optical fiber axis and the particle trajectory, reaching a maximum when the Cerenkov cone is directed along the fiber axis. While Cerenkov radiation is not directly related to radiotherapy dose to the scintillator (Reft, 2006) it can exceed the intensity of the scintillation signal even at the wavelength where the scintillation light is at its most intense. To account for accurate dosimetry, the Cerenkov radiation must be removed from the scintillator signal.

Many methods have been proposed and tested to correct for the effects of Cerenkov light on scintillation dosimetry. Beddar *et al.* used a “background fiber” immediately adjacent to a signal fiber to measure Cerenkov light generated in the background fiber

alone with the assumption that the Cerenkov light generated in the background fiber is the same as in the signal fiber (Beddar et al., 1992). A subtraction was then performed to give the magnitude of scintillation signal. This technique is limited by a consequential disparity in background signal generation in each fiber, particularly in high dose gradient regions. By using a scintillator with a long wavelength emission and filtering out the light with shorter wavelengths, de Boer *et al.* were able to exploit the spectral difference between scintillation light and Cerenkov light to reduce, but not eliminate, contributions of the Cerenkov light to the scintillation signal (de Boer et al., 1992). Unlike de Boer *et al.*, and with the assumption that the spectrum of the Cerenkov background signal is unchanging, in particular, if the Cerenkov spectrum is independent of the electron energy and the angle of incidence on the fiber, Fontbonne *et al.* showed that measurements at two separate wavelengths are sufficient to subtract the Cerenkov background (Fontbonne et al., 2002).

Because radiotherapy beams are typically pulsed, the scintillator signal may be time resolved from the prompt Cerenkov and native fluorescence radiation if the relaxation time of the scintillator is long enough and the dose delivered by the radiotherapy unit in between pulses is negligible. To obtain scintillation signal alone, the time interval when sampling occurs is selected so that it is after the termination of the Cerenkov and native fluorescence radiation-induced signal and before the termination of the scintillation signal. Justus *et al.* (Justus et al., 2004), like Clift *et al.* (Clift et al., 2002), used this concept, however, for  $\text{Cu}^+$ -doped quartz as the radiation-

sensitive element with longer luminescence decay times, rather than a plastic scintillator.

In the current study, the characteristics of a  $\text{Cu}^+$ -doped scintillation detector for clinical electron beams with nominal energy in the range 6–20 MeV were assessed. For 6 MeV beam, measurements were made at seven different dose rates (100 – 1000 MU/min); controlled by the machine pulse rate and not the pulse duration, which remained constant  $\sim 5$  microsecond. Thus, the time interval between pulses ranges between  $\sim 20$  ms (100 MU/min dose rate) and 3 ms (600 MU/min dose rate) during each 5 microsecond duration electron pulse, radioluminescence from the point dosimeter, as well as Cerenkov radiation and native fluorescence from the multimode optical fiber, are excited. The decay of the Cerenkov emission is on the picoseconds time scale and the native fluorescence decays on a nanosecond time scale so that both the Cerenkov and the native fluorescence emissions are immediately terminated after the electro pulse terminates. In contrast, the phosphorescence signal from the  $\text{Cu}^+$ -doped glass persists for several hundred microseconds after the x-ray pulse terminates. Because of the difference in these lifetimes, signals due to Cerenkov and native fluorescence were efficiently separated from the phosphorescence signal between electron pulses by gated detection (Justus et al., 2004). As a consequence of the dose-rate response independence, the reproducibility of the scintillation detector under electron irradiation was examined at 600 MU/min with each measurement representing the integrated charge obtained from an irradiation of 100 MU at standard calibration setting. Standard deviation percentages for signal were contained well

within a 0.55% envelope relative to the average reading. Output signal linearity was tested at a similar dose rate as reproducibility, which was found to be linear for all investigated energies. The  $\text{Cu}^+$ -doped quartz detector demonstrated reproducible dose measurements of electron beams with a linear response to absorbed dose and response independence to dose rate, dose per pulse and energy.

## CHAPTER 7

### CONCLUSION

The FOCDs showed great response for electrons and are recommended for clinical dosimetric use. When placed directly in the electron beam, the FOCDs produced very linear results in comparison with the reference ionization chamber. The only exception was when trying to detect scatter radiation during the TSE commissioning process. The response of each FOCD to each electron beam energy was linear, with computed linearity coefficients with  $R^2$  value = 1.0. The dose rate dependence of the FOCD system at dose rates ranging from 100 to 1000 MU/min was within  $\pm 0.50\%$  of reference ionization chamber measurements and remained uniform well within the reproducibility of the FOCD system. The relative response of the FOCDs for a 6 MeV electron beam is within 0.51% of the reference ionization chamber measurements, except for measurements at 115 cm where the difference was 0.89%.

The ionization ratio of the FOCDs correlated well with that of the reference ionization chamber, and was within  $\pm 1.67\%$  for all the energies investigated, indicating little or no energy dependence. The reproducibility of the FOCD system was within  $\pm 0.55\%$  in solid water at standard calibration settings for a 6 MeV electron beam at 100 MU irradiations. Quantitatively, for electron field size dependence, the maximum difference between the FOCD response and that of the reference ion chamber was within  $\pm 1.69\%$  (6 MeV),  $\pm 0.77\%$  (9 MeV),  $\pm 0.64\%$  (12 MeV),  $\pm 1.46\%$  (16 MeV), and  $\pm 1.55\%$  (20 MeV).

The FOCDs size and ability to relay real time dose information make them highly attractive for clinical radiotherapy. With further research the future of FOCDs in patient care is promising. Maybe with the help of wireless technology such as Bluetooth, the use of FOCDs may be more practical and useful in the treatment environment.

## BIBLIOGRAPHY

AAPM Report 13. Physical Aspects of Quality Assurance in Radiation Therapy.

American Institute of Physics, Inc., New York, NY, 1984.

AAPM Report 23. Total Skin Electron Therapy: Technique and Dosimetry. American

Institute of Physics, Inc., New York, NY, 1998.

AAPM Report 87. Diode in vivo dosimetry for patients receiving external beam radiation therapy. American Association of Physicists in Medicine, College Park, MD,

2005.

Archambault L, Beddar AS, Gingras L, Roy R, Beaulieu L. Measurement accuracy and Cerenkov removal for high performance, high spatial resolution scintillation dosimetry. *Med Phys* 2006;33:128-135.

Ayotte G, Archambault L, Gingras L, Lacroix F, Beddar AS, Beaulieu L. Surface preparation and coupling in plastic scintillator dosimetry. *Med Phys* 2006;33:3519-3525.

Aznar MC, Andersen CE, Botter-Jensen L, et al. Real-time optical-fibre luminescence dosimetry for radiotherapy: physical characteristics and applications in photon beams. *Phys Med Biol* 2004;49:1655-1669.

Beddar AS, Mackie TR, Attix FH. Water-equivalent plastic scintillation detectors for high-energy beam dosimetry: I. Physical characteristics and theoretical consideration. *Phys Med Biol* 1992;37:1883-1900.

Beddar AS, Mackie TR, Attix FH. Cerenkov light in optical fibres and other light pipes irradiated by electron beams. *Phys Med Biol* 1992;37:925-935.

Bogdanich, W. Radiation Offers New Cures, and Ways to Do Harm. New York Times. <file:///C:/Users/Kevin/Documents/OSURHP/Thesis/New%20York%20Times%20Radiation%20article.html>. Retrieved 24, January 2010.

Benevides LA, Huston AL, Justus BL, et al. Characterization of a fiber-optic-coupled radioluminescent detector for application in the mammography energy range. *Med Phys* 2007;34:2220-2227.

Cheung T, Butson MJ, Yu PK. Energy dependence corrections to MOSFET dosimetric sensitivity. *Australas Phys Eng Sci Med* 2009;32:16-20.

Clift MA, Johnston PN, Webb DV. A temporal method of avoiding the Cerenkov radiation generated in organic scintillator dosimeters by pulsed mega-voltage electron and photon beams. *Phys Med Biol* 2002;47:1421-1433.

de Boer SF, Beddar AS, Rawlinson JA. Optical filtering and spectral measurements of radiation induced light in plastic scintillation dosimetry. *Phys Med Biol* 1993;38:945–958.

Fontbonne JM, Iltis G, Ban G, Battala A, Vernhes JC, Tillier J, Bellaize N, Le Brun C, Tamain B, Mercier K, Motin JC. Scintillating fiber dosimeter for radiation therapy accelerator. *IEEE Trans Nucl Sci* 2002;49:2223–2227.

Gaza R, McKeever SWS, Akselrod MS, et al. A fiber-dosimetry method based on OSL from  $\text{Al}_2\text{O}_3:\text{C}$  for radiotherapy applications. *Radiat Meas* 2004;38:809-812.

Gaza R, McKeever SW. A real-time, high-resolution optical fibre dosimeter based on optically stimulated luminescence (OSL) of KBr:Eu, for potential use during the radiotherapy of cancer. *Radiat Prot Dosimetry* 2006;120:14-19.

Hecht, J. City of Light. Oxford University Press, 1999.

Huston AL, Justus BL, Falkenstein PL, *et al.* Remote optical fiber dosimetry. *Nucl Instrum Methods B*, 2001;184:55–67.

Huston AL, Justus BL, Falkenstein PL, *et al.* Optically stimulated luminescent glass optical fiber dosimeter. *Radiat Prot Dosimetry*, 2002;101:23-26.

Hyer DE, Fisher RF, Hintenlang DE. Characterization of a water-equivalent fiber-optic coupled dosimeter for use in diagnostic radiology. *Med Phys* 2009;36:1711-1176.

Justus BL, Falkenstein P, Huston AL, *et al.* Gated fiber-optic-coupled detector for in vivo real-time radiation dosimetry. *Applied Optics* 2004;43:1663-1668.

Justus BL, Falkenstein P, Huston AL, Plazas MC, Ning H, Miller RW. Gated fiber-optic-coupled detector for in vivo real-time radiation dosimetry. *Applied Optics* 2004;43:1663-1668.

Justus BL, Falkenstein P, Huston AL, *et al.* Elimination of Cerenkov interference in a fibre-optic-coupled radiation dosimeter. *Radiat Prot Dosimetry* 2006;120:20-23

Khan, F. The Physics of Radiation Therapy. Lippincott Williams and Wilkins, 2003.

Knoll, G. Radiation Detection and Measurement. John Wiley and Sons, 2000.

Lacroix F, Archambault L, Gingras L, Guillot M, Beddar AS, Beaulieu L. Clinical prototype of a plastic water-equivalent scintillating fiber dosimeter array for QA applications. *Med Phys* 2008;35:3682-3690.

Law SH, Fleming SC, Suchowerska N, McKenzie DR. Optical fiber design and the trapping of Cerenkov radiation. *Appl Opt* 2006;45:9151–9159.

Law SH, Suchowerska N, McKenzie DR, Fleming SC, Lin T. Transmission of Cerenkov radiation in optical fibers. *Opt Lett* 2007;32:1205–1207.

Ramani R, Russel S, O'Brien P. Clinical dosimetry using MOSFETs. *Int J Radiat Oncol Biol Phys* 1997;37:954–64.

Reft C. Radiation characteristics of a gated fiber-optic-coupled detector. *Med Phys* 2006;33:2194-2195.

Tanyi JA, Krafft SP, Hagio T, Fuss M, Salter BJ. MOSFET sensitivity dependence on integrated dose from high-energy photon beams. *Med Phys* 2008;35:39-47.

Tanyi JA, Krafft SP, Ushino T, Huston AL, Justus BL. Performance characteristics of a gated fiber-optic-coupled dosimeter in high-energy pulsed photon radiation dosimetry. *Appl Radiat Isot* 2010;68:364-369.

Thomson I, Thomas RE, Berndt LP. Radiation dosimetry with MOS sensors. *Radiat Prot Dosimetry* 1984;6:121-124.